

Spectroscopic properties of Er^{3+} ions doped in calcium niobium gallium garnet disordered crystals

Taiju TSUBOI¹⁾

Silviu POLOSAN^{1,2)}

Kiyoshi SHIMAMURA³⁾

Hyo-Jin SEO⁴⁾

¹⁾ Faculty of Engineering, Kyoto Sangyo University, Kyoto 603-8555, Japan

²⁾ National Institute of Materials Physics, Bucharest-Magurele, PO Box MG-7, 077125, Romania

³⁾ Optronic Materials Center, National Institute for Materials Science, Tsukuba 305-0044, Japan

⁴⁾ Department of Physics, Pukyong National University, Busan 608-737, Republic of Korea

Abstract

Spectroscopic properties of Er^{3+} -doped and non-doped calcium niobium gallium garnet [$\text{Ca}_3(\text{Nb}_{2-x}\text{Ga}_x)\text{Ga}_3\text{O}_{12}$] disordered crystals have been studied in 200-2000 nm range at 10-290 K in detail, which are compared with the cases of Er^{3+} doped in ordered crystals of LiYF_4 and YAlO_3 . Various emission bands due to Er^{3+} are observed at 350-1600 nm range. From the emission spectra, which are obtained by excitations with lights of various wavelengths, and from the excitation spectra, level assignment has been made for all the emission bands. In addition to sharp absorption and emission lines due to Er^{3+} ions, a broad absorption band is observed at 317 nm at 12 K and a broad emission band is observed at 470 nm. These broad bands are observed in both doped and non-doped crystals.

1. Introduction

Inorganic rare-earth-doped optical materials of crystals, polycrystals and glasses are used for not only scintillators [1] and optical communication fibers [2,3], but also lasers, fluorescent lamps, cathode ray tubes [4] and infrared-to-visible up-convertors [5,6]. Optical properties of rare earth ions have been studied by doping these ions to crystals such as garnets and fluorides. Of various garnets like YAG, calcium niobium gallium garnet $\text{Ca}_3(\text{Nb}_{2-x}\text{Ga}_x)\text{Ga}_3\text{O}_{12}$ (called CNGG,

hereafter) crystal have several advantages because of its non-stoichiometric and disordered crystal structure. For example, lower melting point which makes crystal growth easy, broad absorption and emission bands which make possible more efficient diode-pumping for high-power laser action at room temperature, large concentration of doping rare-earth ions which gives rise to high emission intensity.

Most garnets have $\{\text{X}_3\}[\text{Y}_2](\text{Z}_3)\text{O}_{12}$ structure where X, Y and Z ions occupy the dodecahedral (C), octahedral (A) and tetrahedral (D) sites, respectively. In the case of grossular garnet, $\text{X}=\text{Ca}^{3+}$ (calcium ion), $\text{Y}=\text{Al}^{3+}$ (aluminum) and $\text{Z}=\text{Si}^{3+}$ (silicon ion) i.e., $\text{Ca}_3\text{Al}_2\text{Si}_3\text{O}_{12}$, while in the case of yttrium aluminum garnet (YAG), $\text{X}=\text{Y}^{3+}$ (yttrium ion) and $\text{Y}, \text{Z} = \text{Al}^{3+}$ (aluminum), i.e., $\text{Y}_3\text{Al}_5\text{O}_{12}$. On the other hand, CNGG has $\{\text{Ca}_3\}[\text{Nb}_{2-x}\text{Ga}_x](\text{Ga}_3)\text{O}_{12}$ structure, where $0 < x, z < 1$ [7,8]. Unlike grossular garnet and YAG where all metal ions have trivalent ions, the metal ions have different valence states in CNGG, i.e., Ca^{2+} , Nb^{5+} and Ga^{3+} . Cation vacancies also occupy at the D and A sites. The positions of the metal ions are not uniquely fixed. Such a situation gives rise to structural disorder and presence of various site symmetries around the metal ions, resulting in the broadening of absorption and emission bands of the doped impurity ions such as Er^{3+} with $4f^{11}$ electron configuration [9,10].

Optical and spectroscopic properties of CNGG crystals doped with various rare-earth ions have been studied, for example, Tm^{3+} -doped CNGG [7, 12, 13, 14], Nd^{3+} -doped CNGG [7, 15, 16, 17, 18], Yb^{3+} -doped CNGG [15, 19], Er^{3+} -doped CNGG [11, 20] and Eu^{3+} -doped CNGG [15]. Very few studies have been undertaken for Er^{3+} -doped CNGG when compared with CNGG doped with the other rare-earth ions. In this paper we study the spectroscopic properties, especially absorption and photoluminescence characteristics in visible and near infrared regions at various temperatures between 290 K and 12 K, and clarify the luminescence processes.

So far the broadening is observed for various rare-earth ions doped in CNGG at room temperature. We are interested in the following question: whether the spectral broadening is characteristics of disordered CNGG crystal? For this purpose we compare the spectra of Er^{3+} ion in CNGG at low temperature such as 12 K with the spectra of Er^{3+} ion in ordered crystals.

2. Experimental procedure

The Er^{3+} -doped calcium niobium gallium garnet structure $\text{Ca}_3(\text{NbGa})_{2-x}\text{Ga}_3\text{O}_{12}$ crystals were grown by Czochralski method using a standard rf-heating furnace and iridium crucible. The raw material consists of a mixture of CaCO_3 , Nb_2O_5 and Ga_2O_3 with ratio of 36.472:242.36:36.286 (wt%) and dopant powder of Er_2O_3 . In the crystal growth process, a mixture of inert gases O_2 and N_2 was

used in order to avoid the evaporation of gallium oxides from the melt. Single crystal of CNGG doped with 3.04 wt% Er^{3+} ions and non-doped CNGG crystal were grown.

Absorption and magnetic circular dichroism (MCD) spectra were measured with a Cary 5E spectrophotometer and a Jasco J-40A polarimeter, respectively, at 290 and 12 K. Luminescence spectra were measured with a Spex Fluorolog-3 spectrophotometer using 450 W Xe-lamp at various temperatures between 12 and 300 K. UV-visible-near infrared emission was detected with a Hamamatsu Photonics R928 photomultiplier tube with sensitivity at 250-850 nm, while infrared emission was detected with an Electro-Optical Systems thermoelectrically cooled DSSX-IGA020E InGaAs photodiode with sensitivity at 800-1700 nm. In the luminescence measurements, slit widths of the emission and excitation monochromators were set as 0.3 nm to get highly resolved spectra.

3. Experimental Results

Figure 1 shows the absorption spectra of Er^{3+} -doped CNGG crystal at 12 K and room temperature, together with non-doped CNGG crystal. Absorption bands due to the transitions from the $^4\text{I}_{15/2}$ ground state to the $^4\text{I}_{13/2}$, $^4\text{I}_{11/2}$, $^4\text{I}_{9/2}$, $^4\text{F}_{9/2}$, $^4\text{S}_{3/2}$, $^2\text{H}_{11/2}$, $^4\text{F}_{7/2}$, $^4\text{F}_{5/2}$, $^4\text{F}_{3/2}$, $^2\text{H}_{9/2}$, $^4\text{G}_{11/2}$, $^2\text{G}_{9/2}$, $^2\text{K}_{15/2}$, $^2\text{G}_{7/2}$, $^2\text{P}_{3/2}$ and $^4\text{G}_{7/2}$ excited states in Er^{3+} appear at about 1443-1627, 957-1040, 783-808, 644-660, 539-558, 513-537, 482-499, 449-459, 440-445, 403-411, 374-389, 365-369, 362-365, 355-359, 316-318 and 293.1 nm at room temperature, respectively. Each of these bands consists of several sharp lines. Absorption band due to the transition to the $^2\text{K}_{13/2}$ state is expected to appear at about 300 nm, but it was too weak to observe clearly even at 12 K.

When temperature is decreased from room temperature to 12 K, weak absorption bands at low-energy in each band decreases and disappears at 12 K. Examples are shown in Figs. 2 and 3 for the absorption bands associated with the $^4\text{I}_{13/2}$ and $^4\text{I}_{9/2}$ states, respectively, where the weak bands observed at 1543-1627 and 986-1040 nm at 290 K disappear at 12 K.

Intense absorption due to band-to-band transition of CNGG host begins from 297 nm. A broad absorption band is observed at 317 nm in both the doped and non-doped crystals, which is superimposed on the band-gap absorption. The peak of this band shifts from 325 nm to 317 nm as temperature is decreased from 290 K to 12 K.

Magnetic circular dichroism (MCD) absorption signals are observed for each absorption band as shown in Fig. 4. The MCD signal is S-shape for the $^4\text{F}_{9/2}$, $^4\text{F}_{7/2}$, $^4\text{F}_{5/2}$, $^4\text{F}_{3/2}$, $^2\text{H}_{9/2}$ and $^2\text{G}_{7/2}$ bands, while reversed S-shape for the $^4\text{S}_{3/2}$, $^2\text{H}_{11/2}$, $^4\text{G}_{11/2}$, $^2\text{G}_{9/2}$ and $^2\text{K}_{15/2}$ bands. The MCD intensity is nearly proportional to the absorption intensity.

When Er^{3+} -doped CNGG crystal is excited at 376 nm (corresponding to the excitation into the $^4\text{G}_{11/2}$ state), emission bands are observed at about 403-420, 515-535, 540-565, 645-682, 790-830, 840-870, 960-1040, 1220-1260 and 1440-1545 nm at room temperature. These emission bands are shown in Figs. 5-12 at various temperatures between 290 K and 12 K. As seen in Fig. 5, unlike the case of emission from the $^2\text{H}_{9/2}$ state, emission due to the transitions from the $^4\text{F}_{7/2}$, $^4\text{F}_{5/2}$, $^4\text{F}_{3/2}$ states to the ground state is not observed. Unlike the cases of excitation at 375 and 543 nm, the infrared emission bands at 840-870 and 1220-1260 nm are not observed by excitation at 667 nm as shown in Fig. 12. This is confirmed by the excitation spectra for the 840-870 and 1220-1260 nm emissions (Fig. 13). The 1440-1545 nm emission band is generated by not only the 375, 543, 667 nm excitations but also 285 and 320 nm excitations. It is noted that this 1440-1545 nm emission band range becomes narrow (1525-1545 nm) with decreasing temperature as seen in Fig. 9.

From the excitation at various wavelengths, it is concluded that the two infrared emission bands at 840-870 and 1220-1260 nm are caused by the transition from the $^4\text{S}_{3/2}$ state as shown in Fig. 14. The intensities of the 840-870 and 1220-1260 nm emission bands increase with decreasing temperature (Figs. 9 and 10). Such an increase of emission intensity is also observed for the 645-682 nm emission band (Fig. 7). On the other hand, in the 960-988, 998-1040 and 1440-1550 nm emission bands, the intensities of their high-energy bands decrease with decreasing temperature and their low-energy bands become sharp (Fig. 9).

The absorption band associated with the $^2\text{H}_{11/2}$ state, which appears at 515-538 nm, is much more intense than the absorption band associated with the $^4\text{S}_{3/2}$ state, which appears at 540-565 nm. However, the emission band associated with the $^2\text{H}_{11/2}$ state is much weaker than the emission band associated with the $^4\text{S}_{3/2}$ state, and the former band decreases with decreasing temperature, while the latter band enhances as shown in Fig. 6. Figure 15 plots these intensities against temperature. The increase of emission intensity continues up to about 100 K and stops below 100 K for the 540-565 nm band, while the decrease of intensity continues up to the same temperature (about 100 K) and stops below 100 K for the 515-538 nm band. This indicates that the two bands have strong correlation to each other.

When Er-doped CNGG crystal is excited with 285 nm light corresponding to the energy gap of CNGG, a broad emission band with a peak at 470 nm is observed in addition to the sharp bands due to Er^{3+} (Fig. 16). Several dips are observed in the 470 nm broad emission band at 375-525 nm range. Their peak wavelengths and intensity ratios are the same as the Er^{3+} absorption bands shown in Fig. 1. Therefore the dips are due to self-absorption by Er^{3+} . The 470 nm emission band enhances with decreasing temperature. The 470 nm emission band has an excitation band with a peak at 280 nm. The same results are obtained in non-doped CNGG as shown in Figs. 17 and 18.

Therefore it is concluded that the 470 nm emission is due to CNGG host. The excitation into the 280 nm absorption band also gives rise to the Er^{3+} emission, and additionally the excitation spectrum for 470-480 nm emission consists of not only the 280 nm band but also the Er^{3+} absorption bands associated with corresponding to $^2\text{P}_{3/2}$, $^2\text{K}_{13/2}$, $^2\text{D}_{7/2}$ and $^2\text{D}_{5/2}$ excited states (Fig. 19).

As seen in Fig. 19, absorption band associated with $^2\text{P}_{3/2}$ state has a peak at 314.7 nm, absorption band associated with $^2\text{K}_{13/2}$ state has two peaks at 304.7 and 300.7 nm, absorption band associated with $^2\text{D}_{7/2}$ state has a peak at 292.0 nm, and absorption band associated with $^2\text{D}_{5/2}$ state has a peak at 286.0 nm, which are not observed in usual absorption spectra of Fig. 1 because of intense absorption due to host CNGG. Same excitation spectrum as Fig. 19 was obtained for 403, 527, 543 and 670 nm Er^{3+} emissions.

When Er-doped CNGG crystal is excited with 317 nm light to give rise to excitation into the $^2\text{P}_{3/2}$ state, emission bands which are not observed by the 376 nm excitation are observed at 527.3, 532.1, 472.6, 403, 372.7, 366.4 nm, etc. at 12 K as shown in Fig. 20. These emissions are attributed as follows ; 527.3, 532.1 nm: $^2\text{P}_{3/2} \rightarrow ^4\text{I}_{9/2}$, 472.6 nm: $^2\text{P}_{3/2} \rightarrow ^4\text{I}_{11/2}$, 403 nm : $^2\text{P}_{3/2} \rightarrow ^4\text{I}_{13/2}$, 372.7 nm : $^4\text{G}_{11/2} \rightarrow ^4\text{I}_{15/2}$, 366.4 nm: $^2\text{G}_{9/2} \rightarrow ^4\text{I}_{15/2}$ (see Fig. 14). The same emission spectrum as Fig. 20 was also obtained by 295 nm excitation.

Figure 21 shows temperature dependence for the intensities (band areas) of the four infrared emission bands that are observed by 376 nm excitation. The emission bands at 840-870 and 1220-1260 nm increase with decreasing temperature as the case of the 645-682 nm emission band, while the emission bands at 960-1040 and 1440-1550 nm decrease.

The emission band at 540-565 nm consists of two bands. One is at 540-548 nm, and the other is at 550-565 nm. These two bands show the same temperature dependence to each other (Fig. 6), indicating they arise from the same origin. The same is true for the emission band at 1220-1260 nm (Fig. 10), band at 840-875 nm (Fig. 11), and also band at 645-682 nm (Fig. 22).

The high-energy component at 987-973 nm in the 950-1050 nm emission band (Fig. 12) is drawn in energy scale of [cm^{-1}] in Fig. 23, and compared with the high-energy component at 650-660 nm in the 645-682 nm band (Fig. 7). These spectra are drawn in the same 300 cm^{-1} range. Quite similar line shape is observed between the two bands. The 987-973 nm emission is due to the transition from the $^4\text{I}_{11/2}$ state to the ground state, and the 650-660 nm emission from the $^4\text{F}_{9/2}$ state to the ground state. The ground state is common to the two emissions. Therefore it is suggested that the line shape of Fig. 23 reflects the energy state of the ground state.

The emission spectrum at 950-1050 nm consists of two emission bands, one has a peak at about 976 nm and the other has a peak at 1003 nm (Fig. 9). It is possible to assign the two band to different origins from comparison of energy level diagram of Er^{3+} , e.g. the former band to $^4\text{I}_{11/2} \rightarrow$

⁴I_{15/2}, the latter to ⁴F_{7/2} → ⁴I_{15/2}. However, the excitation into the ⁴F_{9/2} state (which locates at lower energy than the ⁴F_{7/2} state) with 660 nm light and excitation with lights of wavelengths shorter than 520 nm give the same spectra. Therefore it is concluded that the two bands arise from the same ⁴I_{11/2} → ⁴I_{15/2} transition. The two bands arise from the Stark splitting of the ⁴I_{11/2} state. The separation of the bands is about 275 cm⁻¹. Such a 275 cm⁻¹ separation is not observed in the other emission bands.

4. Discussion

4.1. Temperature dependence of the ⁴S_{3/2} and ²H_{11/2} emission bands

Interesting temperature dependence is observed for the luminescence of Er³⁺ in not only infrared PL bands but also visible PL bands. For example, the intensity of the 540-565 nm ⁴S_{3/2} emission band increases with decreasing temperature, while the 515-538 nm ²H_{11/2} emission band decreases and almost disappears below 100 K as shown in Fig. 6. We explain this temperature dependence by solving the rate equations for the two energy states of ²H_{11/2} and ⁴S_{3/2}. A numerical calculation was undertaken by taking into account the non-radiative one-phonon relaxation process between the ²H_{11/2} and ⁴S_{3/2} states (see inset of Fig. 15). The rate equations for the populations of these states are given by as follows.

$$\frac{dN_2}{dt} = -k_{21}N_2 - k_2N_2 + k_{12}N_1$$

$$\frac{dN_1}{dt} = +k_{21}N_2 - k_{12}N_1 - k_1N_1$$

$$\text{where } k_{12} = \frac{1}{e^{\Delta E / kT} - 1} K \quad k_{21} = \left(\frac{1}{e^{\Delta E / kT} - 1} + 1 \right) K$$

Parameters N₂ and N₁ (k₂ and k₁) are the populations (radiative transition rates) of the levels ²H_{11/2} and ⁴S_{3/2}, respectively. K is the coupling constant between those two levels and ΔE is the energy difference between levels. The k₁₂ and k₂₁ are the non-radiative phonon transition rates between the two levels. The initial conditions are N₂ (t=0) = 1 and N₁ (t=0) = 0.

We neglected the non-radiative transition from the ⁴S_{3/2} state to the nearest lower-energy ⁴F_{9/2} state because the gap energy is about 3100 cm⁻¹ that does not allow the multi-phonon transitions by taking into account gap law and the phonon energy 362 cm⁻¹ [10] of CNGG. Photoluminescence lifetime of the ⁴S_{3/2} → ⁴I_{15/2} transition has two components in Er³⁺-doped CNGG, i.e., a fast decay component of 15.1 μs and the slow component of 30.5 μs [11]. Therefore we use the inverse of 15.1 μs as k₁. The energy gap between the ²H_{11/2} and ⁴S_{3/2} levels were estimated as

675 cm⁻¹ at 12 K from the absorption spectra and we use this value as ΔE . Good fitting between the measured and calculated PL intensities of the two emission bands was obtained by choosing values of $k_1=6.25 \times 10^4$ s⁻¹, $k_2=1.4 \times 10^5$ s⁻¹, $K=12 \times 10^7$ s⁻¹, as shown by solid lines in Fig. 15. The radiative lifetime of 0.7 μ s estimated for the ²H_{11/2} state is reasonable because it is much shorter than the lifetime of the forbidden ⁴S_{3/2} state. From this result, we confirm that the thermal activation from the lower ⁴S_{3/2} state induces the emission from the upper ²H_{11/2} state.

The fast depopulation in the ²H_{11/2} level and the increase of population in the ⁴S_{3/2} level are confirmed from the temperature dependences of the other emission bands. For example, the 1240 and 860 nm emission bands, which are attributed to the ⁴S_{3/2}→⁴I_{11/2} and ⁴S_{3/2}→⁴I_{13/2} transitions (Fig. 14), respectively, enhance with decreasing temperature. This is consistent with the enhancement of the 540-565 nm ⁴S_{3/2} emission.

4.2. Broad absorption and emission bands

Broad absorption band is observed at about 317 nm at 12 K and at 325 nm at 290 K. This band is observed not only Er³⁺-doped CNGG but also non-doped CNGG, indicating that this band is due to CNGG host. The excitation at 317 nm does not give rise to any broad emission band in non-doped CNGG even at low temperatures, but gives rise to sharp Er³⁺ emission bands in the doped CNGG. Energy transfer occurs from the host to Er³⁺ dopant. Two models are conceivable as the origin of the 317 nm absorption band. The first is a charge-transfer band, the second is trapped center which is formed by oxygen vacancy in disordered CNGG. It is suggested that the lack of emission by the 325 nm excitation in non-doped CNGG is due to intersystem crossing in which the luminescence is quenched.

Two broad bands have been observed at 330 and 440 nm in Ce³⁺-doped and non-doped LaBr₃ crystals, that have the same excitation band at 230 nm [21]. The broad bands have been attributed to bound electron-hole pairs of host lattice [21]. The 230 nm excitation band is located close to the band gap of LaBr₃ host. Similar characteristics are found for the broad emission band with a peak at 470 nm and its excitation band at 280 nm in Er³⁺-doped and non-doped CNGG crystals. Therefore the 470 nm emission of CNGG is attributed to bound electron-hole pair of CNGG host. Additionally broad absorption band is observed at 325 nm in both the doped and non-doped CNGG. It locates at lower energy side but very close to the band gap. Taking into account that disordered CNGG has cation vacancies, it is suggested that the 325 nm absorption band is attributable to creation of exciton near the cation-vacancy defect [1].

4.3. Comparison with Er^{3+} -doped YLF and YAlO_3 ordered crystals

We compare the absorption and photoluminescence spectra of Er^{3+} ions between disordered crystal of CNGG and ordered crystals of LiYF_4 (called YLF) and yttrium aluminium perovskite YAlO_3 , to check how much band broadening appears in CNGG disordered crystal. LiYF_4 is a tetragonal crystal of the Scheelite structure. Er^{3+} ions substitute for the Y^{3+} ions without charge compensation. On the other hand, YAlO_3 is a biaxial crystal of orthorhombic structure with four molecules per unit cell. The space group is Pbnm. Er^{3+} ions enter the Y^{3+} lattice sites having a Cs point symmetry.

Figure 24 shows the absorption spectra of Er^{3+} -doped CNGG and YAlO_3 at 12 K. Broadening is found for each absorption band in CNGG crystal. It is noted that the absorption coefficient of CNGG is higher by about five times for each band than that of YAlO_3 , indicating more efficiently absorbed in CNGG than YAlO_3 . This is understood as follows. The local symmetry of Er^{3+} in disordered crystal is more lower than the ordered YAlO_3 , giving rise to stronger mixing of the parity-allowed f^0d states to the parity-forbidden f^1 state. As a result, the absorption intensity becomes higher in CNGG than in YAlO_3 .

The emission bands, which are due to the transitions from the $^4\text{S}_{3/2}$ and $^2\text{H}_{11/2}$ states to the ground state, are shown for Er^{3+} -doped CNGG, YLF and YAlO_3 crystals in Fig. 25. The band consists of many lines. More highly resolved spectra are obtained in YLF and YAlO_3 than in CNGG. The same is true for the other emission bands, for example as shown in Figs. 26 and 27, where the emission bands due to the transitions from the $^4\text{S}_{3/2}$ state to the $^4\text{I}_{11/2}$ states and from the $^4\text{I}_{13/2}$ state to the ground state at room temperature are presented. Figure 28 shows the emission band due to the transitions from the $^4\text{S}_{3/2}$ state to the ground state at 12 K. Relatively lowly resolved spectrum is also observed for CNGG. The same is clearly observed for the 12 K infrared emission bands as shown in Figs. 29 and 30. Such lowly resolved spectra of disordered CNGG crystal are caused by overlapping among the emission lines of Er^{3+} ions with various site symmetries.

Figure 31 shows the Er^{3+} emission spectra of CNGG and YLF excited at 376 nm at room temperature. The infrared emission was measured under the same experimental conditions (i.e., almost the same concentration of 3.0 % Er^{3+} ions for the two crystals, intensity of excitation light, slit widths of the excitation and emission monochromators, etc.). It is found that the emission intensity is much higher in CNGG than in YLF. This is consistent with the result of Fig. 24 that the disordered CNGG crystal has higher transition probability than the ordered crystal.

References:

- [1] E.V.D. van Loef, P. Dorenbos, C.W.E. van Eijk, K.W. Kramer, H.U. Gudel, Phys. Rev. B 68, 045108 (2003).

- [2] W.A. Clarkson, N.P. Barnes, P.W. Turner, J. Nilsson, D.C. Hanna, *Opt. Lett.* 27, 1989 (2002), W.J. Miniscalco, *IEEE J. Lightwave Technol.* LT-9, 234 (1991).
- [3] M. Foroni, F. Poli, A. Cucinotta, and S. Selleri, *Opt. Lett.* 31, 3228 (2006), D. C. Jones, C. D. Stacey, and A. M. Scott, *Opt. Lett.* 32, 466 (2007).
- [4] S. Shionoya, W.M. Yen, *Phosphor Handbook*, CRC Press New York, 1998.
- [5] F. Gan, Y.H. Chen, *Opt. Mater.* 2, 45 (1993).
- [6] Y.F. Ruan, X.M. Wang, T. Tsuboi, *J. Alloys Comp.* 275/277, 246 (1998).
- [7] K. Shimamura, K. Timosheckin, T. Sasari, K. Hoshikawa, T. Fukuda, *J. Cryst. Growth* 128, 1021 (1993).
- [8] Y. Ono, K. Shimamura, Y. Morii, T. Fukuda, T. Kajitani, *Physica B* 213/214, 420 (1995).
- [9] K. Shimamura, P. Becker, B. Wyncke, F. Brehat, T. Fukuda, C. Carabatos-Nedelec, *J. Phys. Condens. Matter* 10, 6865 (1998).
- [10] R. Balda, J. Fernandez, M. A. Illaramendi, *Phys. Rev. B* 48, 9279 (1993).
- [11] T. Tsuboi, K. Shimamura, T. Fukuda, *Phys. Stat. Sol. (b)* 214, 479 (1999).
- [12] T. Tsuboi, M. Tanigawa, K. Shimamura, *Opt. Commun.* 186, 127 (2000).
- [13] A.A. Kaminskii, E.L. Belokoneva, A.V. Butashin, K. Kurbanov, A.A. Markosyan, S.E. Sarkisov, *Izvestiya Akadem. Nauk SSSR, Inorganic Mater.* 22, 1061 (1985).
- [14] Yu. K. Voronko, S.B. Gessen, N.A. Eskov, P.A. Ryabochkina, A.A. Sobol, S.N. Ushavkov, L.I. Tsymbal, *Quantum Electron.* 23, 39 (1993).
- [15] Yu. K. Voronko, A.A. Sobol, S.N. Ushavkov, *Inorganic Mater.* 38, 390 (2002).
- [16] Yu. K. Voronko, A.A. Sobol, A.Ya. Karasik, N.A. Eskov, P.A. Ryabochkina, S.N. Ushavkov, *Opt. Mater.* 20, 197 (2002).
- [17] A. Brenier, G. Boulon, K. Shimamura, T. Fukuda, *J. Cryst. Growth* 204, 145 (1999).
- [18] A. Lupei, V. Lupei, L. Gheorghe, L. Rogobete, E. Osiac, A. Petraru, *Opt. Mater.* 16, 403 (2001).
- [19] Yu. K. Voronko, A.V. Popov, A.A. Sobol, S.N. Ushavkov, *Inorganic Mater.* 42, 1133 (2006).
- [20] Yu. K. Voronko, S.B. Gessen, N.A. Eskov, V.V. Osiko, A.A. Sobol, S.N. Ushavkov, L.I. Tsymbal, *Sov. J. Quantum Electron.* 20, 643 (1990).
- [21] P. Dorenbos, E.V.D. van Loef, A. P. Vink, E. Van der Kolk, C.W.E. van Eijk, K.W. Kramer, H.U. Gudel, W.M. Higgins, K.S. Shah, *J. Lumin.* 117, 147 (2006).

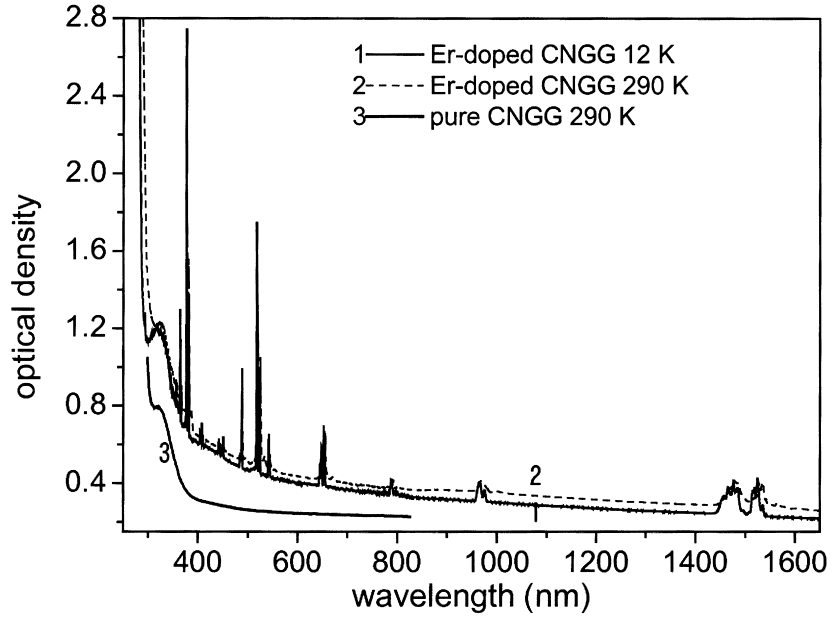


Fig. 1 Absorption spectra of Er^{3+} -doped and non-doped CNGG crystals at 12 K and 290 K.

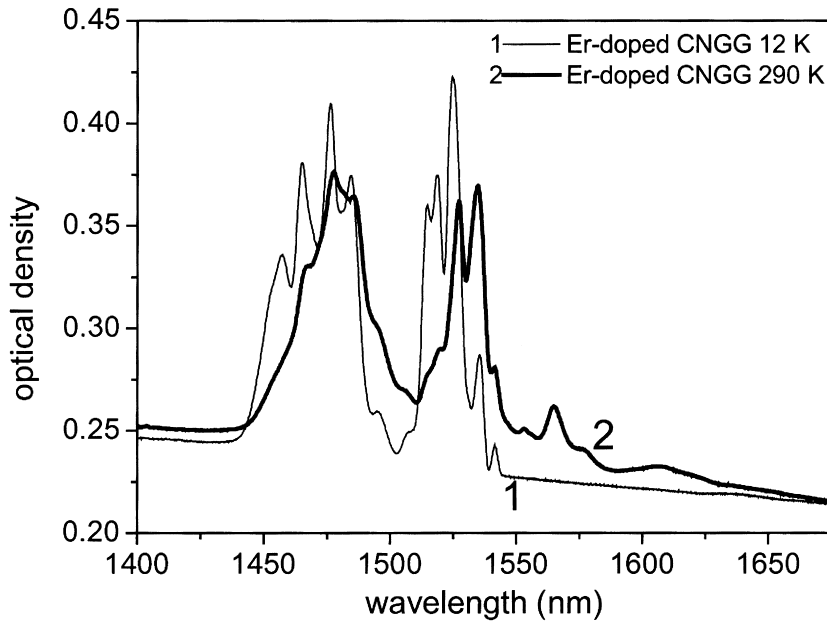


Fig. 2 Absorption spectra, in 1400-1655 nm range, of Er^{3+} -doped CNGG at 12 and 290 K.

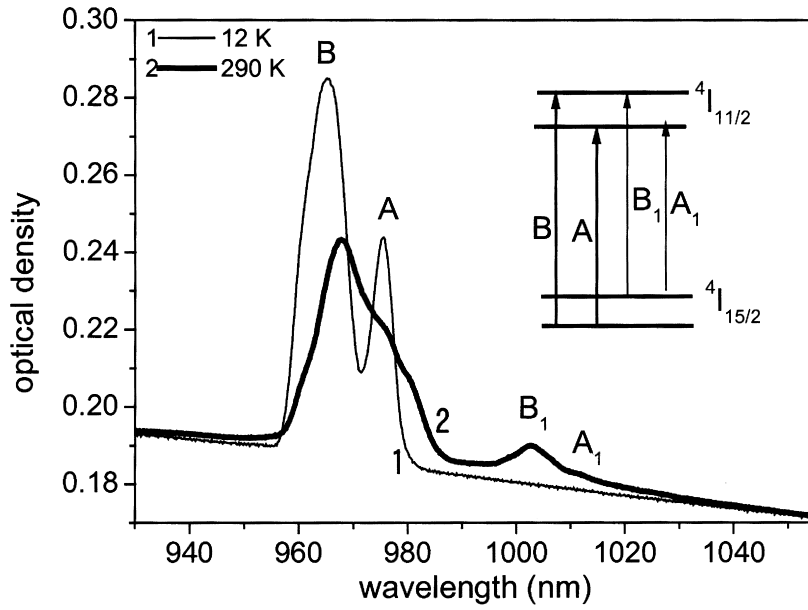


Fig. 3 Absorption spectra, in 960–1040 nm range, of Er³⁺-doped CNGG at 12 and 290 K. Inset shows the absorption processes for the four observed bands.

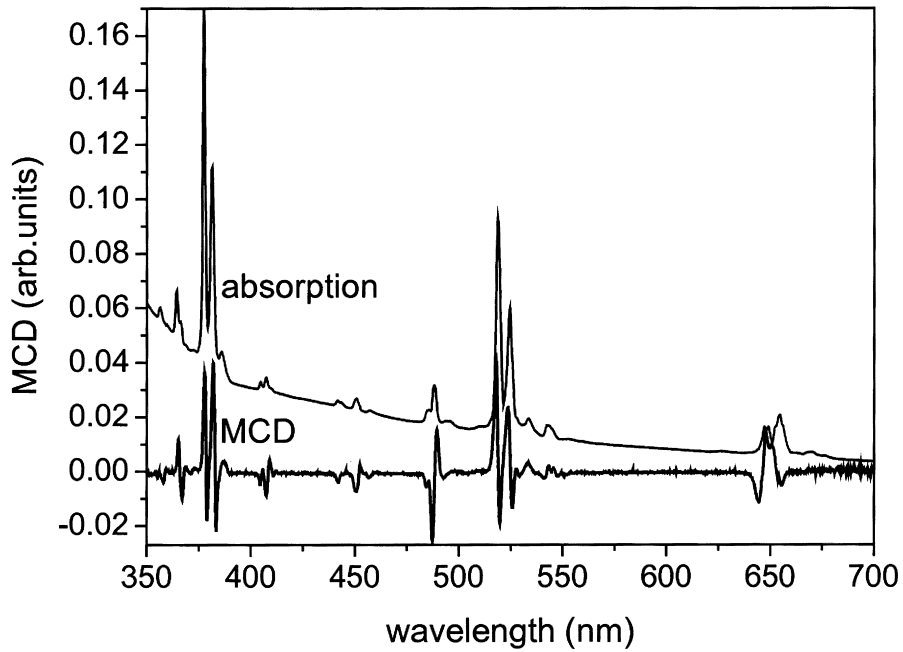


Fig. 4 Magnetic circular dichroism (MCD) absorption of Er³⁺-doped CNGG at 290 K, compared with absorption spectrum at 290 K. MCD was measured under applied magnetic field of 10 kG.

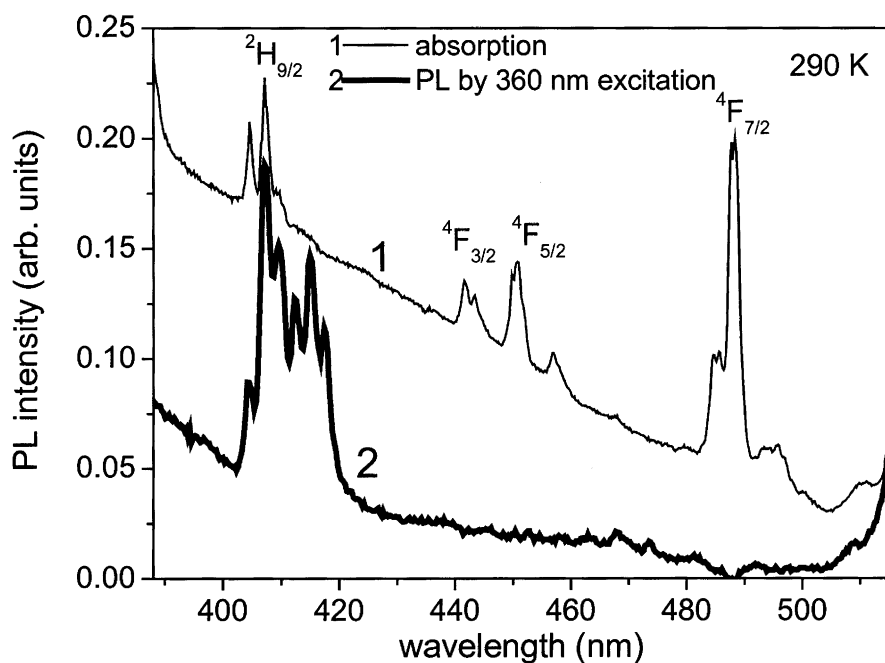


Fig. 5 Emission spectrum (curve 2), in 390-510 nm range, of Er^{3+} -doped CNGG excited at 360 nm at 290 K, compared with the absorption spectrum (curve 1) at 290 K.

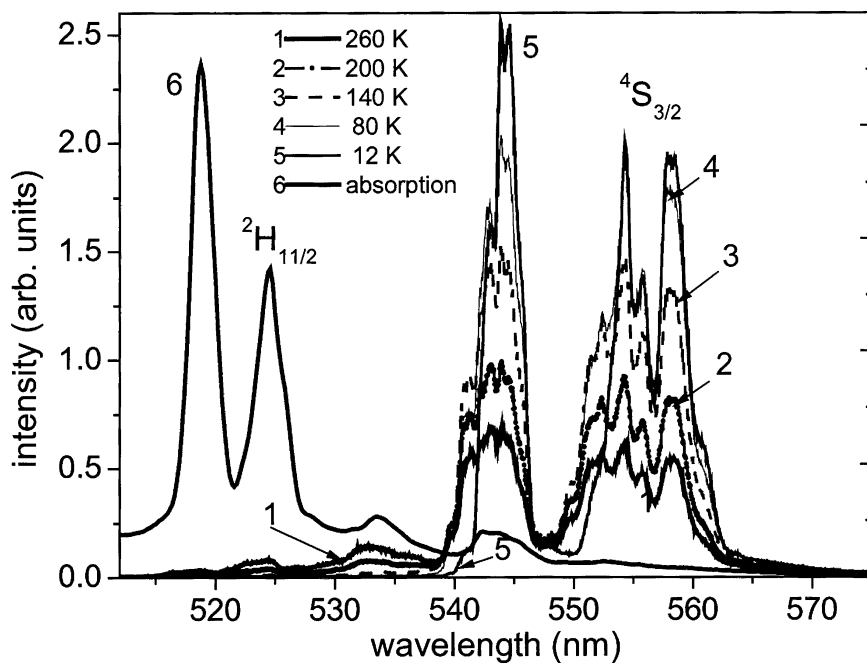


Fig. 6 Temperature dependence of the 510-565 nm emission spectra in Er^{3+} -doped CNGG excited at 376 nm, compared with absorption spectrum at 290 K.

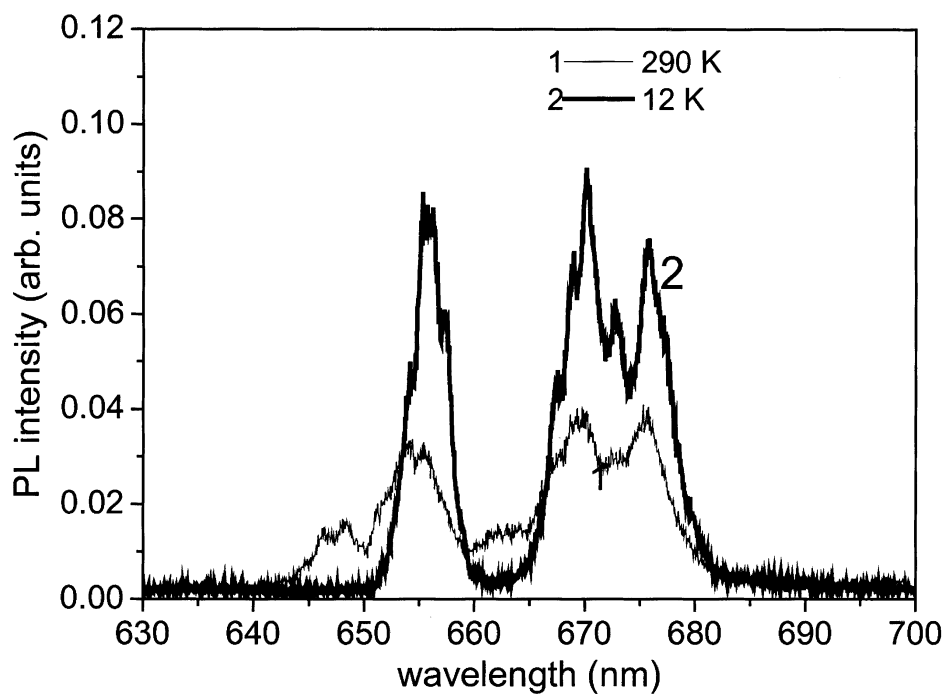


Fig. 7 Emission spectra, in 640-685 nm range, of Er³⁺-doped CNGG excited at 376 nm at 12 and 290 K.

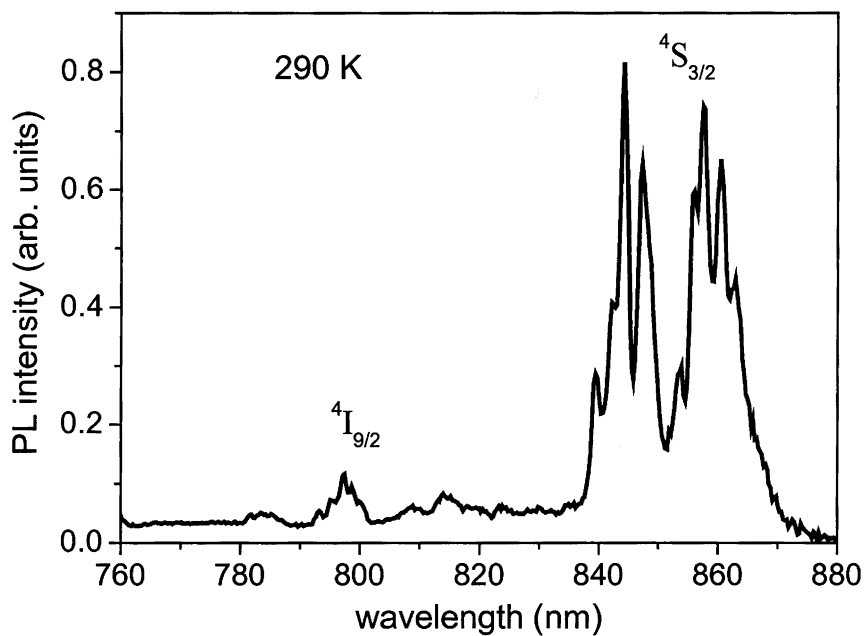


Fig. 8 Near-infrared emission spectrum of Er³⁺-doped CNGG excited at 360 nm at 290 K.

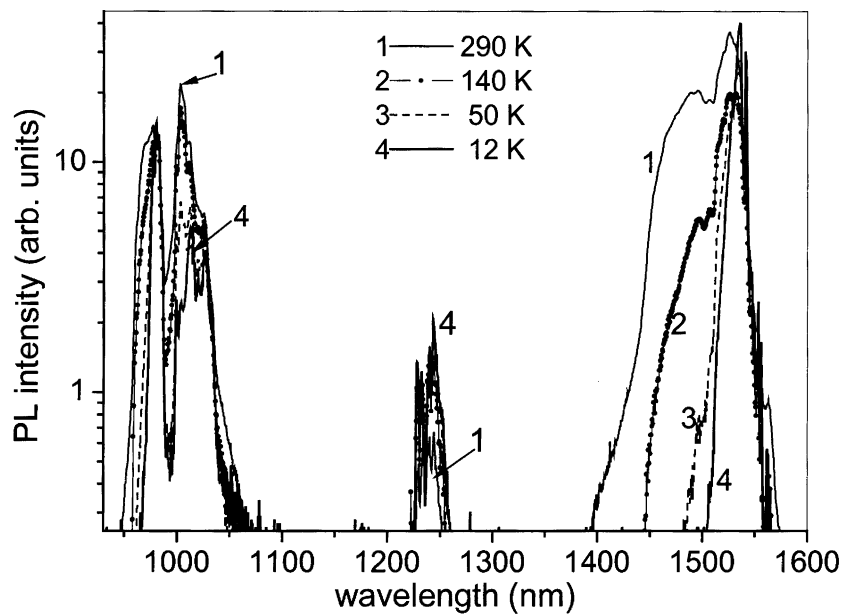


Fig. 9 Temperature dependence of the infrared emission spectra in Er^{3+} -doped CNGG excited at 376 nm.

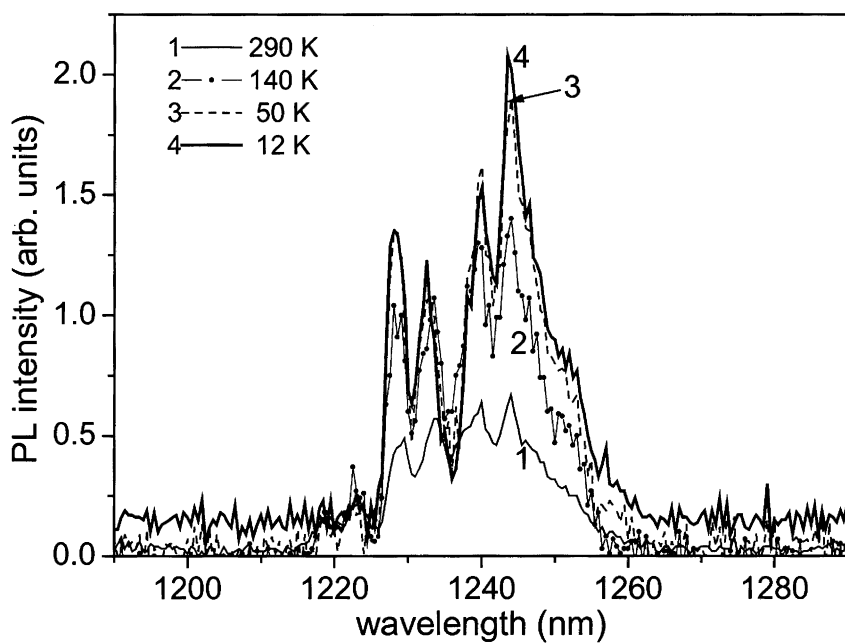


Fig. 10 Temperature dependence of the 1220-1265 nm infrared emission spectra in Er^{3+} -doped CNGG excited at 376 nm.

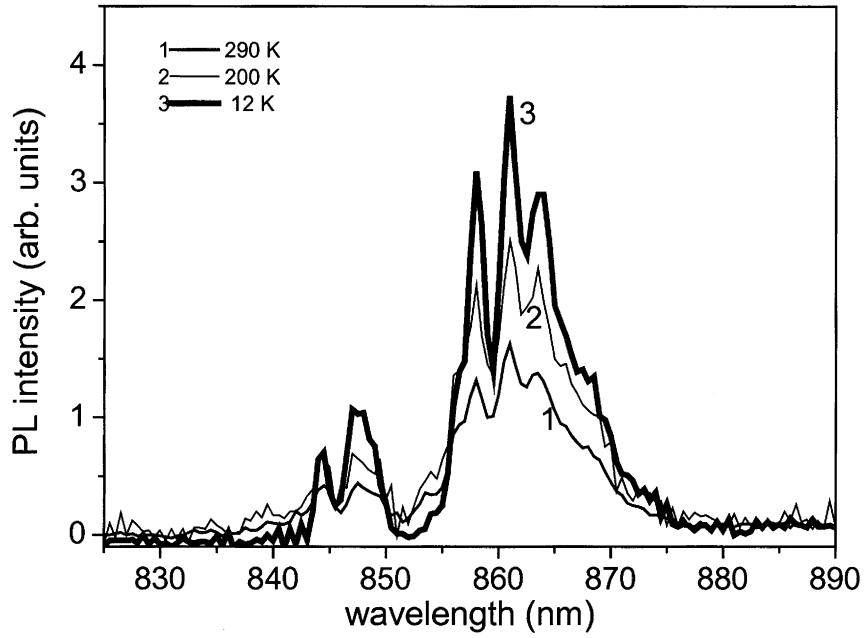


Fig. 11 Temperature dependence of the 840-875 nm infrared emission spectra in Er^{3+} -doped CNGG excited at 376 nm.

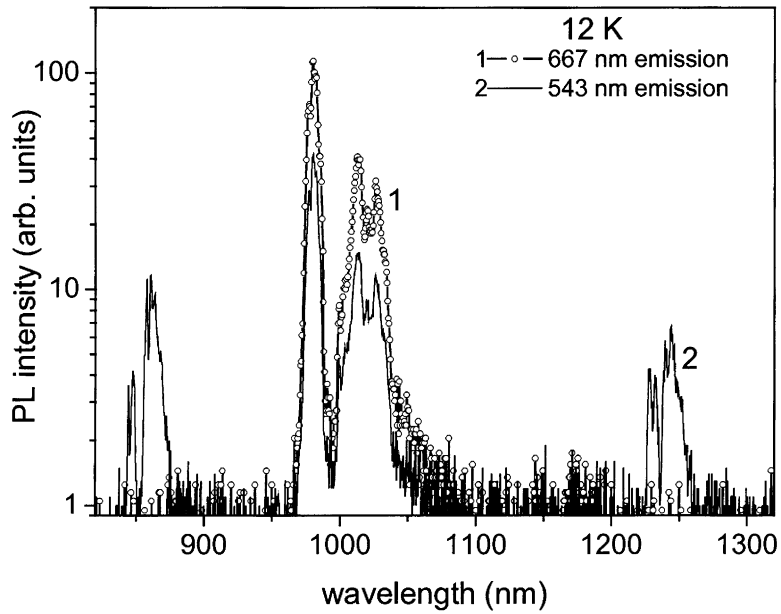


Fig. 12 Near infrared photoluminescence of Er^{3+} -doped CNGG at 12 K for 667 nm (curve 1) and 543 nm (curve 2) emissions, measured with a spectral resolution of 0.2 nm.

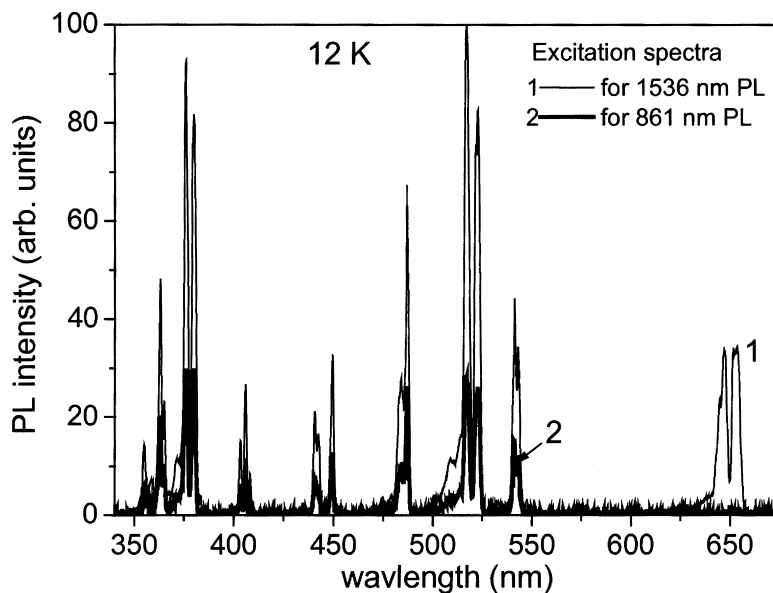


Fig. 13 Excitation spectra for 1536 and 861 nm emissions at 12 K. The same spectra are obtained between the spectra for the 1536 and 980 nm emissions, and between the spectra for the 861 and 1243 nm emissions. The same is true at room temperature.

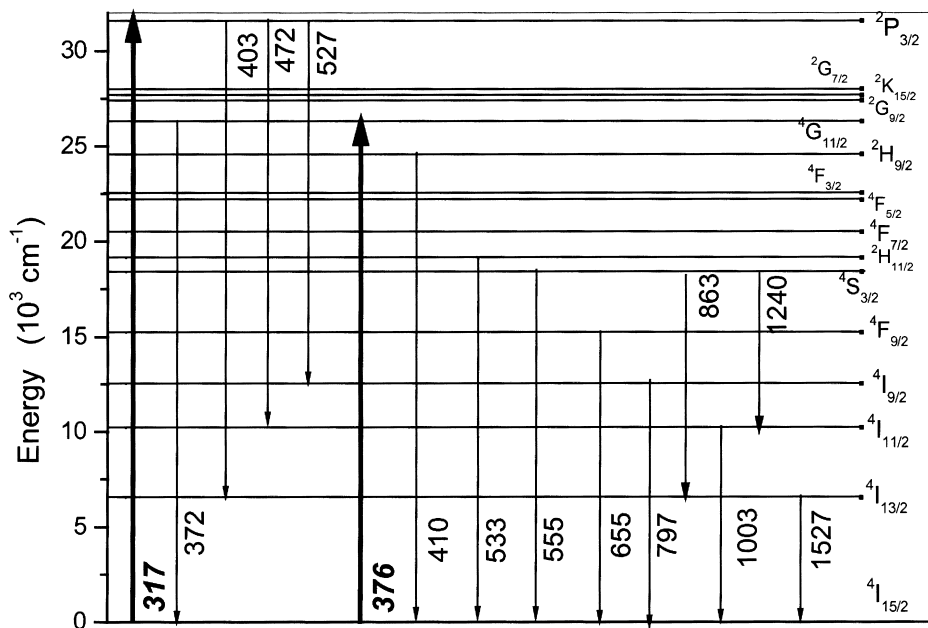


Fig. 14 Level assignment of the emission bands of Er^{3+} in CNGG excited at 376 nm and 317 nm. Numbers of italic letters mean the excitation wavelengths in unit of nm. Each of emission bands consists of several sharp lines. The numbers shown in the diagram indicate wavelength of one of these sharp lines for convenience.

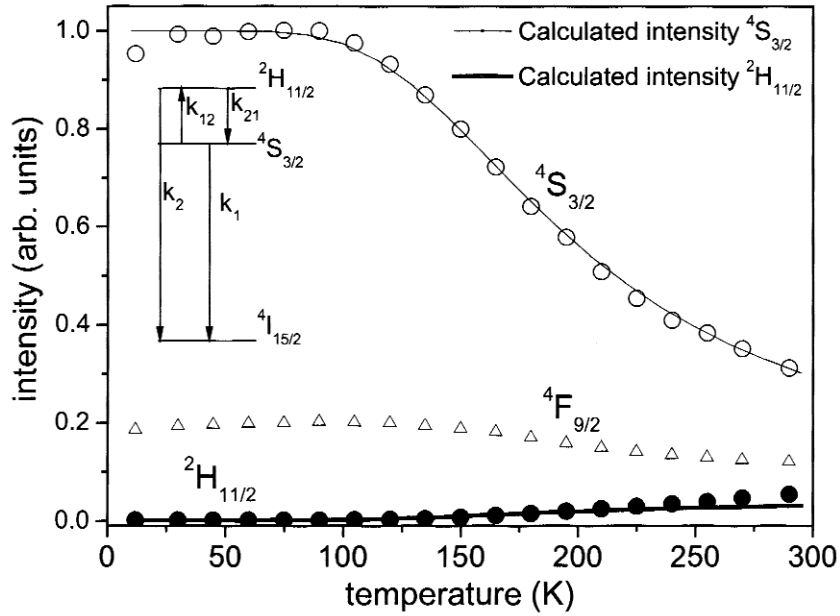


Fig. 15 Temperature dependence of the intensities (integrated areas) of the $^2H_{11/2}$ emission bands at 515-538 nm (closed circles), the $^4S_{3/2}$ emission band at 540-565 nm (open circles) and the $^4F_{9/2}$ emission band at 645-682 nm (open triangles). Solid lines show the calculated results. Inset shows a schematic diagram describing the relaxation and radiative processes of the $^2H_{11/2}$ and $^4S_{3/2}$ emitting states.

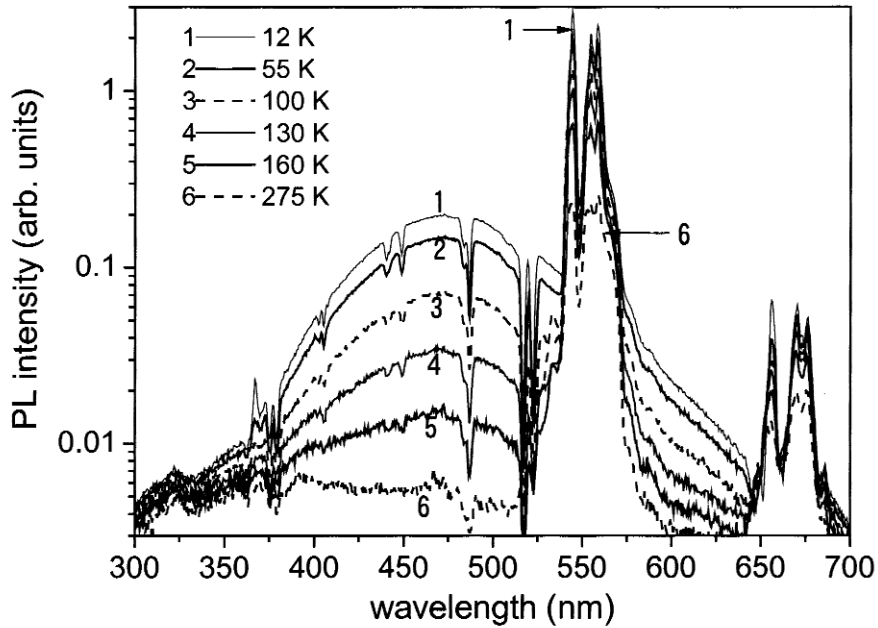


Fig. 16 Temperature dependence of the emission spectra in Er^{3+} -doped CNGG excited at 280 nm.

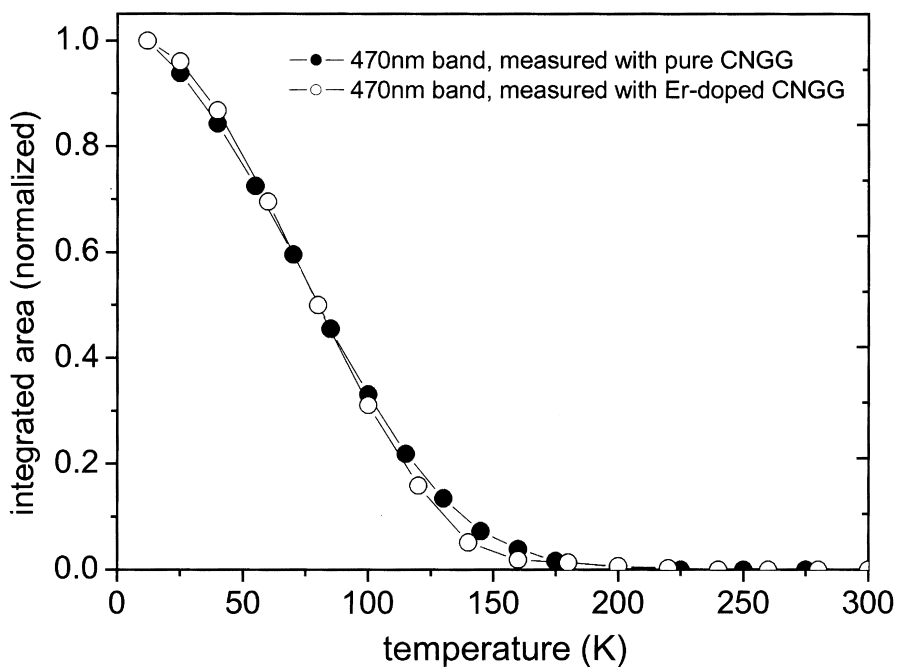


Fig. 17 Temperature dependence of the 470 nm emission band intensity (integrated area) obtained in non-doped CNGG (closed circle) and Er^{3+} -doped CNGG (open circle), which were excited at 285 nm.

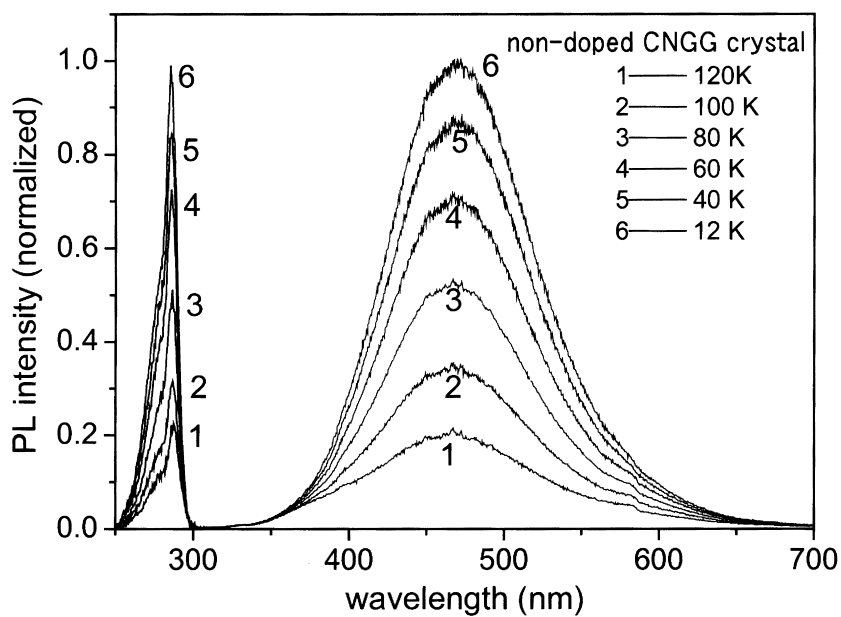


Fig. 18 Emission spectra of non-doped CNGG crystal excited at 287 nm and its excitation spectra for 470 nm emission at various temperatures.

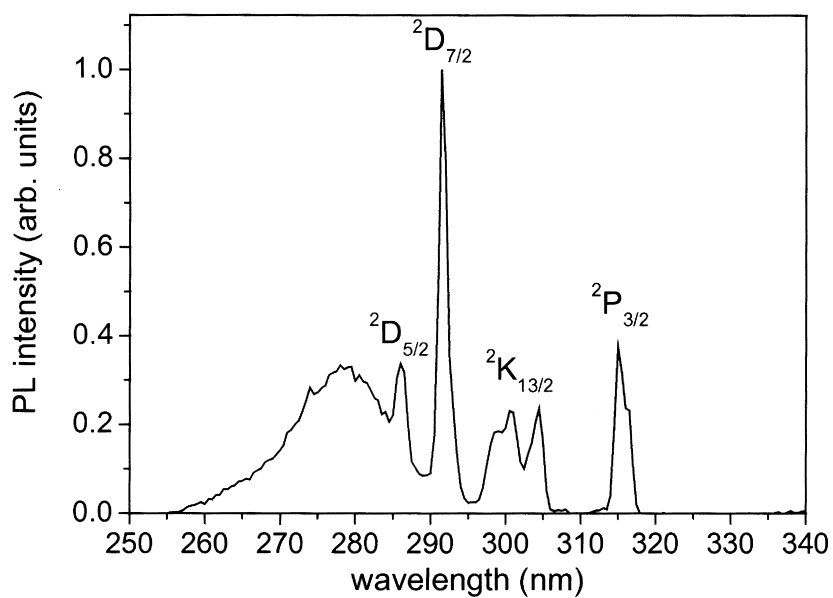


Fig. 19 Excitation spectrum, in 255-340 nm range, for 473 nm emission of Er³⁺-doped CNGG at 12 K.

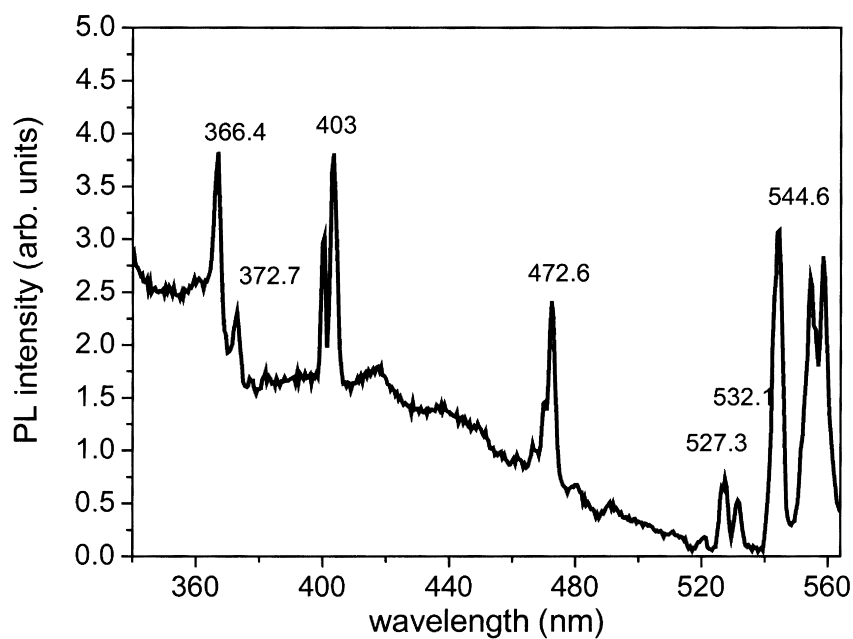


Fig. 20 Emission spectrum, in 350-560 nm range, of Er³⁺-doped CNGG excited at 317 nm at 12 K.

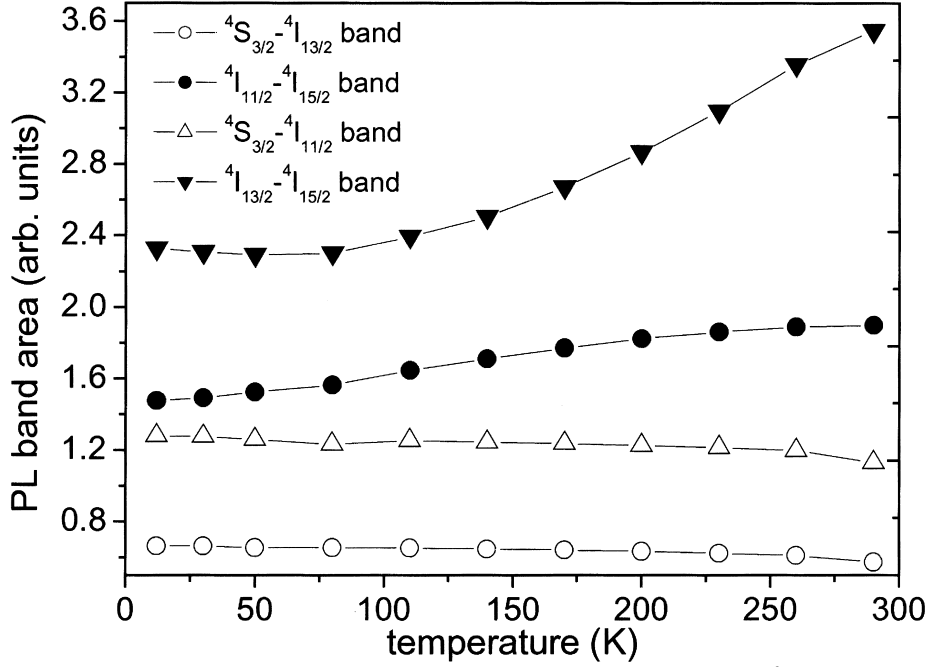


Fig. 21 Temperature dependence of intensity (integrated area) of four infrared Er^{3+} emission bands in CNGG excited at 376 nm.

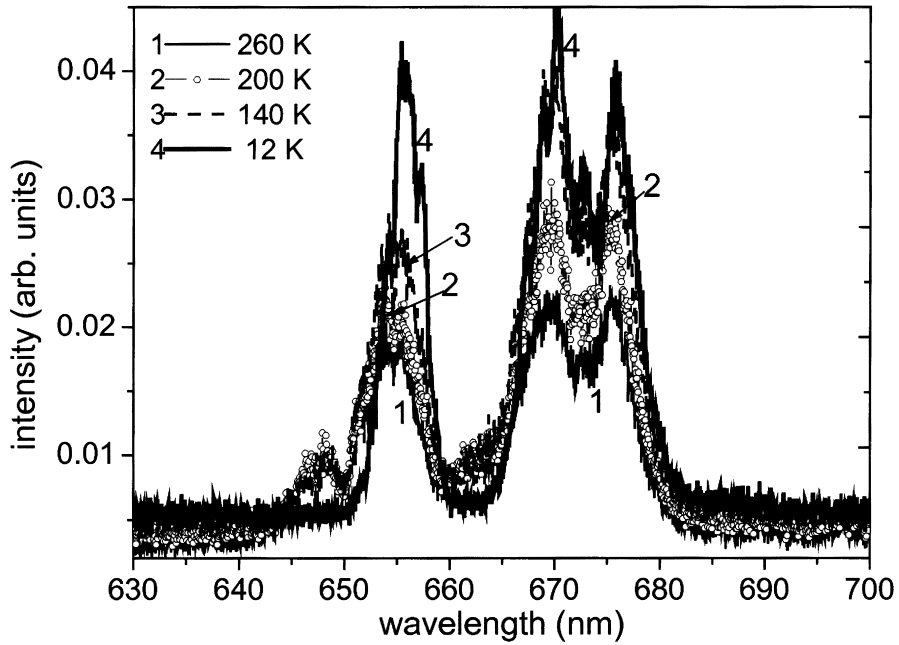


Fig. 22 Temperature dependence of Er^{3+} emission bands at 630-700 nm range, in Er^{3+} -doped CNGG excited at 376 nm.

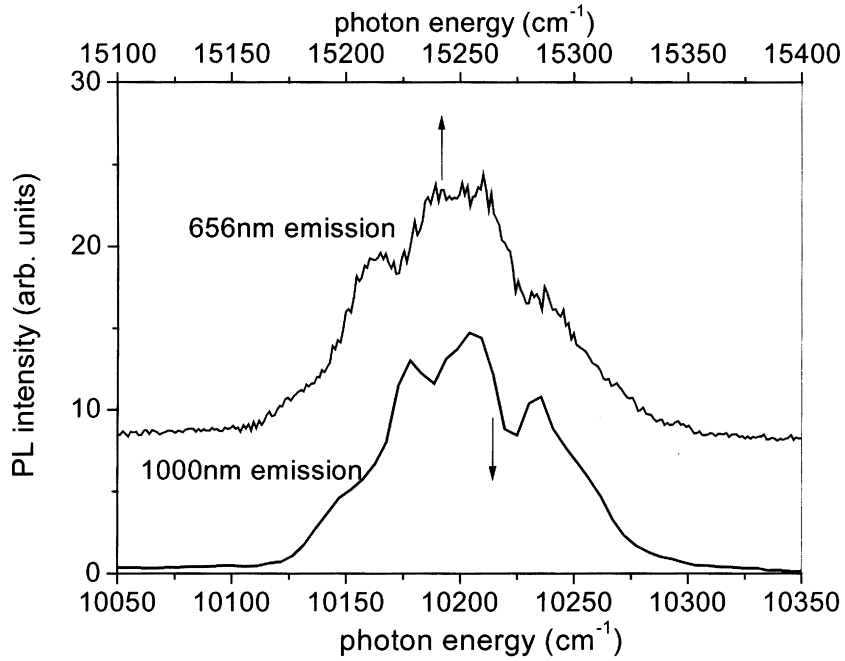


Fig. 23 Comparison of the 1000 and 656 nm emission bands observed at 12 K, which are drawn in the same energy scale. The energy scale for the 656 nm band is shown by upper x-axis, while the scale for the 1000 nm band by the lower x-axis.

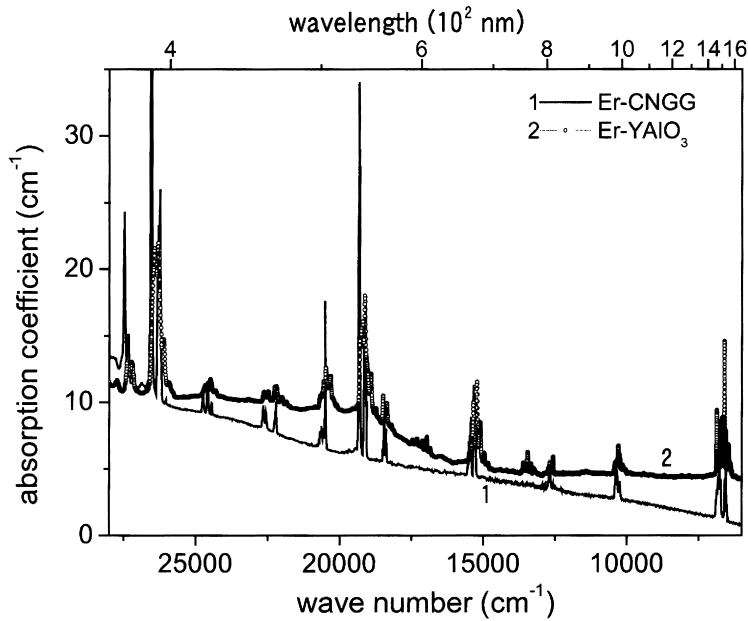


Fig. 24 Absorption spectra of Er³⁺-doped CNGG and Er³⁺-doped YAlO₃ at 12 K. The spectrum of latter crystal is enlarged by five times.

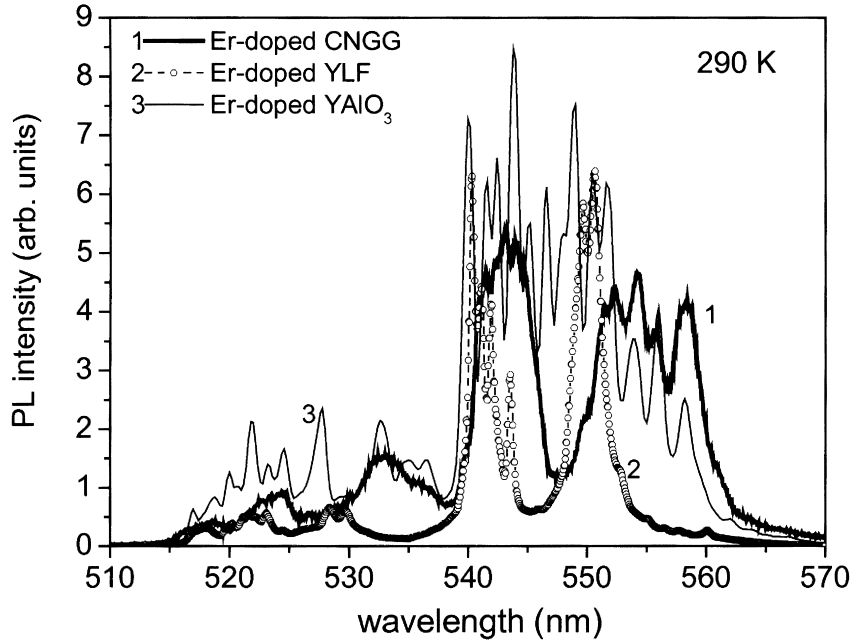


Fig. 25 Emission spectra, in green range, of 3 wt% Er^{3+} -doped CNGG (curve 1), 1 wt% Er^{3+} -doped LiYF_4 (YLF, curve 2) and 3 wt% Er^{3+} -doped YAlO_3 (curve 3) crystals excited at 376 nm at 290 K.

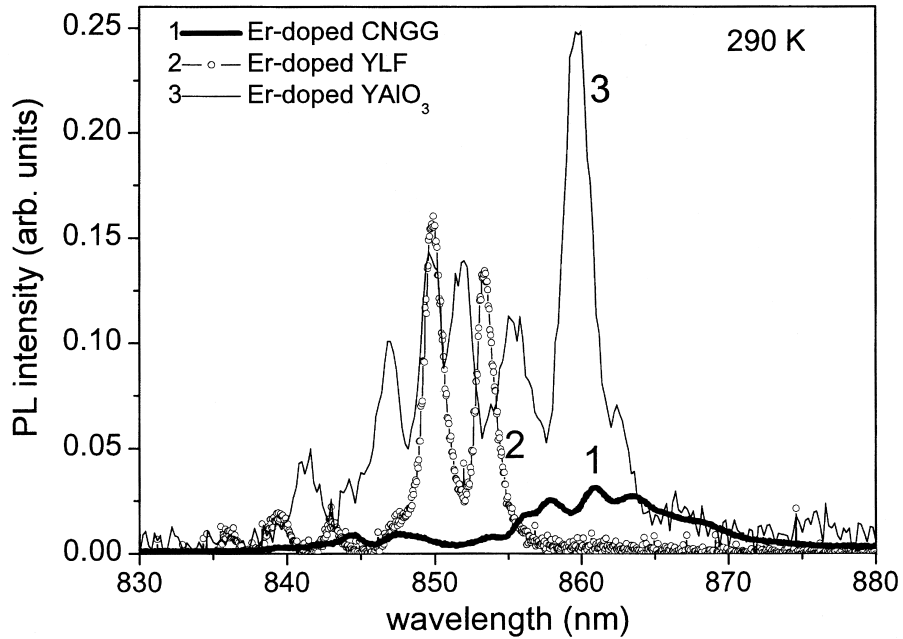


Fig. 26 Emission spectra, in near-infrared range, of Er^{3+} -doped CNGG, LiYF_4 (YLF) and YAlO_3 crystals excited at 376 nm at 290 K. Measurement was made under the same condition as used to obtain Fig. 25.

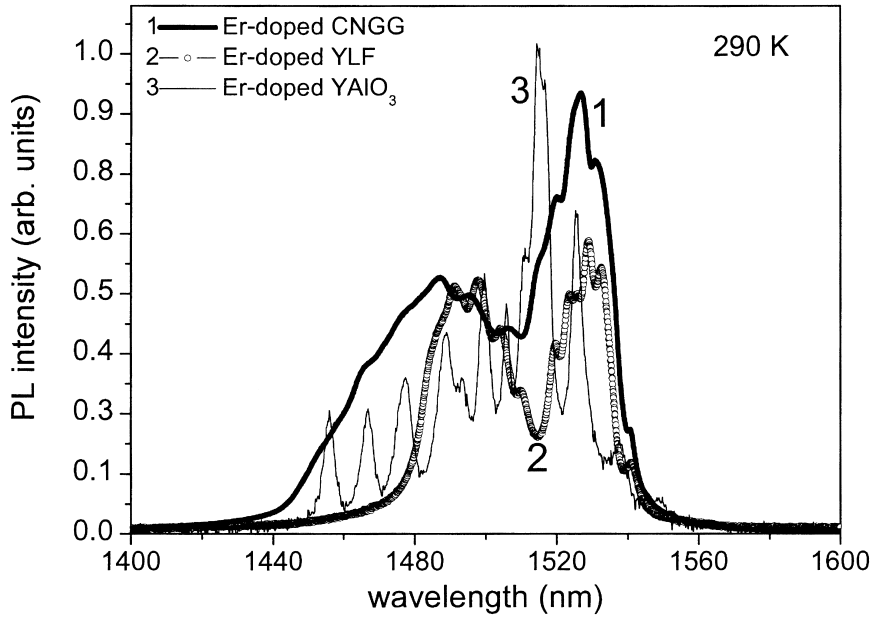


Fig. 27 Emission spectra, in 1400-1550 nm range, of Er³⁺-doped CNGG, LiYF₄ (YLF) and YAlO₃ crystals excited at 376 nm at 290 K. Measurement was made under the same condition as used to obtain Fig. 25.

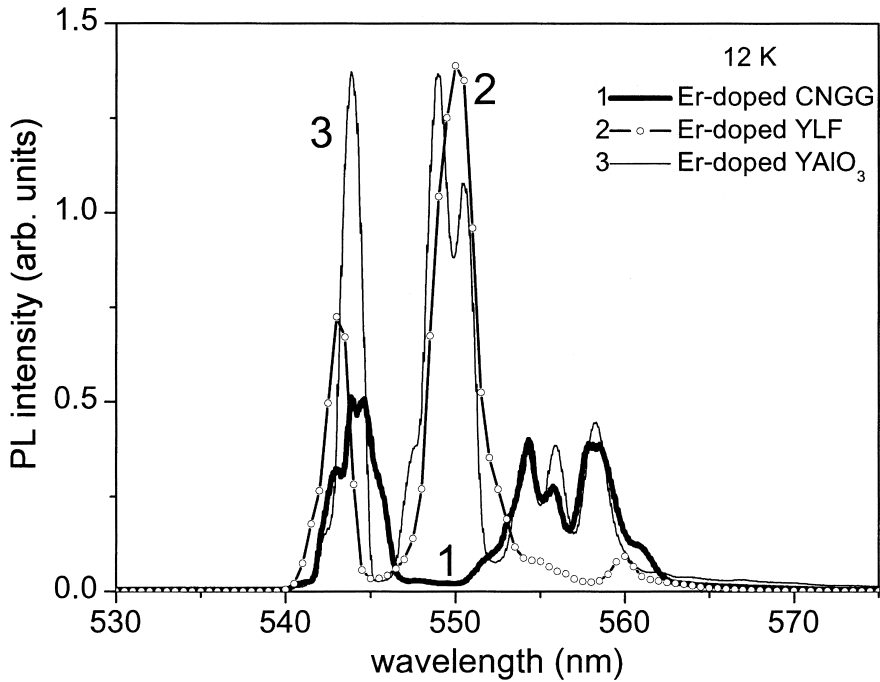


Fig.28 Emission spectra, in green range, of Er³⁺-doped CNGG, LiYF₄ (YLF) and YAlO₃ crystals excited at 376 nm at 12 K.

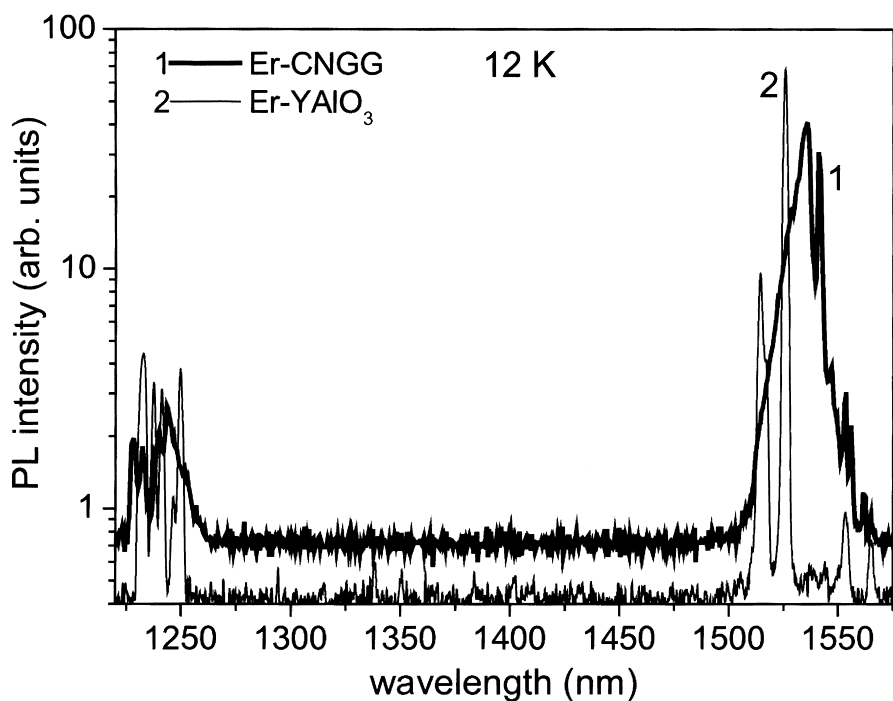


Fig.29 Emission spectra, in infrared range, of Er^{3+} -doped CNGG and YAIO_3 crystals excited at 380 nm at 12 K.

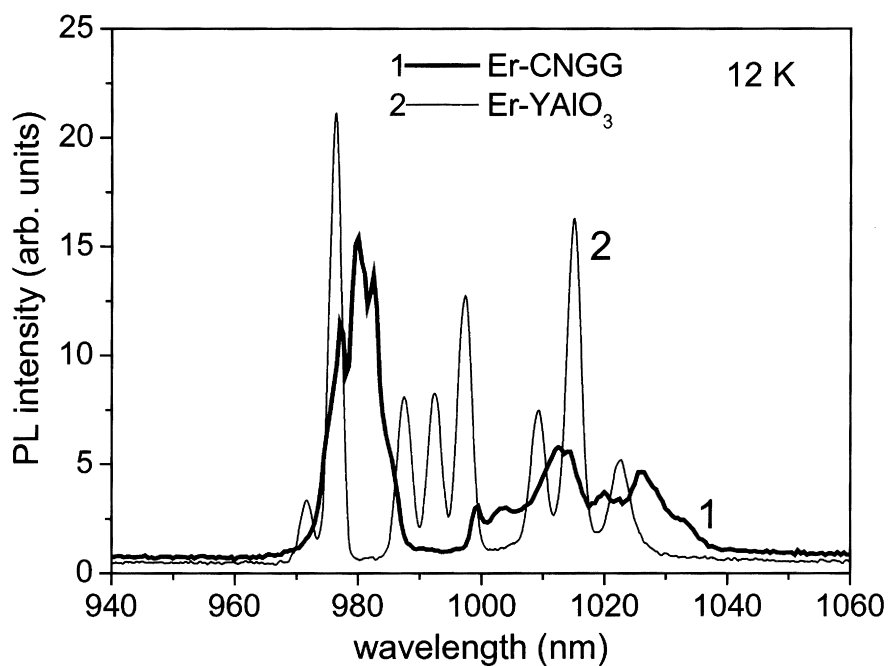


Fig. 30 Emission spectra, in near-infrared range, of Er^{3+} -doped CNGG and YAIO_3 crystals excited at 380 nm at 12 K.

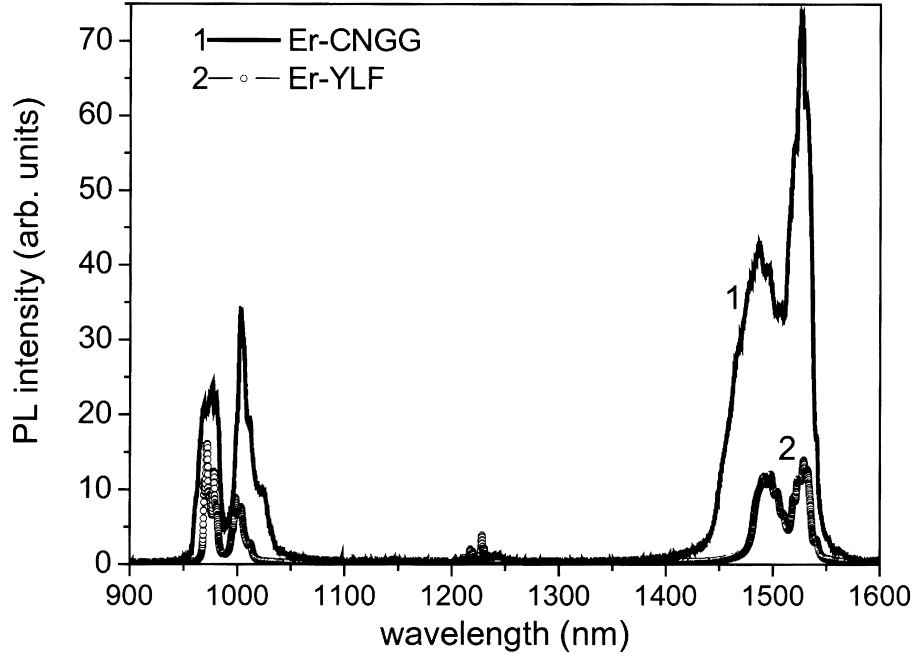


Fig. 31 Emission spectra, in infrared range, of Er^{3+} -doped CNGG and LiYF_4 (YLF) crystals excited at 376 nm at 290 K. The spectra of the two crystals were measured under the same measurement conditions.

